



# Resonant triad interactions of two acoustic modes and a gravity wave

E. Zuccoli<sup>1</sup>  and U. Kadri<sup>1</sup>

<sup>1</sup>School of Mathematics, Cardiff University, Cardiff CF24 4AG, UK

**Corresponding author:** Usama Kadri, [kadriu@cardiff.ac.uk](mailto:kadriu@cardiff.ac.uk)

(Received 2 September 2024; revised 20 January 2025; accepted 20 January 2025)

---

The interaction between acoustic and surface gravity waves is generally neglected in classical water-wave theory due to their distinct propagation speeds. However, nonlinear dynamics can facilitate energy exchange through resonant triad interactions. This study focuses on the resonant triad interaction involving two acoustic modes and a single gravity wave in water of finite and deep depths. Using the method of multiple scales, amplitude equations are derived to describe the spatio-temporal behaviour of the system. Energy transfer efficiency is shown to depend on water depth, with reduced transfer in deeper water and enhanced interaction in shallower regimes. Numerical simulations identify parameter ranges, including resonant gravity wavenumber, initial acoustic amplitude and wave packet width, where the gravity-wave amplitude is either amplified or reduced. These results provide insights into applications such as tsunami mitigation and energy harnessing.

**Key words:** nonlinear dynamical systems, waves/free-surface flows, acoustics

---

## 1. Introduction

Classical water-wave theory neglects the effects of water compressibility due to the different time scales involved in the propagation of both acoustic and surface gravity waves. In the ocean, as well as in the atmosphere, the speed of sound usually far exceeds the propagation speed of the surface gravity waves; hence, acoustic modes are often ignored and only surface gravity waves are taken into consideration. The aforementioned scenario develops in a linear framework when there is no mutual interaction between the two sets of waves. However, when nonlinearity comes into play, interactions between acoustic and gravity waves may no longer be neglected due to the comparable time or

length scales over which their dynamics occurs. This coupling allows for energy exchange among a small number of linear modes and occurs through a resonant triad interaction.

Resonant triad interaction has been studied extensively in different contexts, as well as for various physical systems. Initially, this approach was used to describe the nonlinear interaction between gravity and capillary waves (Wilton 1915; Mcgoldrick 1965; Simmons 1969; McGoldrick 1970; Schwartz & Vanden-Broeck 1979; Hammack & Henderson 1993) and that involving purely gravity waves in specific configurations (Phillips 1960; Benney 1962; Hasselmann 1962; Longuet-Higgins 1962; Miles 1976; Durey & Milewski 2023). Later on, the mechanism of resonant triad interaction was applied to other types of waves, such as those occurring in two-layer flows (Ball 1964; Joyce 1974; Segur 1980), atmospheric flows (Raupp *et al.* 2008; Raupp & Silva Dias 2009) and flexural-gravity waves (Wang *et al.* 2013).

Within the context of a compressible ocean and acoustic–gravity waves, nonlinear resonances have been previously studied in a seminal paper by Longuet-Higgins (1950), followed by Kadri & Stiassnie (2013) and Yang *et al.* (2018), focusing on the numerical calculations of specific triads responsible for the nonlinear resonances, without deriving the nonlinear dynamics of the system. Only in Kadri & Akylas (2016) and later in Kadri & Wang (2021) the nonlinear contribution up to cubic terms was discussed. These studies consider the interaction of two gravity waves with a single acoustic wave.

A triad interaction involving two acoustic modes and a single gravity wave is also possible, as discussed in Kadri (2016, 2017), who considered the deep-water limit. These two studies accounted for nonlinearities up to quadratic terms. However, Kadri & Akylas (2016) demonstrated that cubic nonlinearities also influence the nonlinear evolution of wave amplitudes. Therefore, in this work, we include cubic terms in a comprehensive mathematical model, even though their impact appears negligible. Moreover, we extend the work of Kadri (2016, 2017) by including a shallow-water limit and study the energy exchange in detail. The main goal is to establish a mathematical framework for deriving the nonlinear amplitude equations, and conduct a parametric study to identify energy exchange conditions.

For the derivation of the amplitude equations we employ the same method as used by Kadri & Akylas (2016). The method takes inspiration from the method of multiple scales and allows one to exploit a separation of scales already occurring in the corresponding linear problem. The derived equations are described by a set of nonlinear partial differential equations whose unknowns represent the amplitude of the two acoustic modes and that of the single gravity mode. In addition to the standard quadratic interaction terms analysed in depth in Kadri & Stiassnie (2013), our asymptotic analysis considers the effect of cubic terms in both the governing equation and the free-surface boundary condition, which are found negligible under the considered time and length scales. On the other hand, we find that as the water depth increases, the energy transferred to the gravity mode from the acoustic modes decreases, whereas in shallower regimes, the energy transfer is more efficient. It is also notable that the energy transfer becomes significantly larger when interaction comprises higher acoustic modes. In this case, the amplitude of the gravity mode can increase up to almost twice the maximum amplitude achieved for lower acoustic mode numbers, ultimately reaching a steady state where the aforementioned increased amplitude remains constant in time.

## 2. Preliminaries

Consider a free-surface gravity–acoustic wave disturbance propagating in a slightly compressible water of constant depth  $h$  over a rigid bottom ( $z = -h$ ), under the joint

effects of gravity and compressibility. The motion is assumed irrotational and the water is treated as an inviscid barotropic fluid with a constant sound speed,  $c = (dp/d\rho)^{1/2}$ . Under oceanic conditions where  $h \sim \mathcal{O}(10^3)$  m and  $c = 1.5 \times 10^3$  m s<sup>-1</sup>, a key parameter that controls the effects of gravity relative to compressibility is  $\mu = gh/c^2 \ll 1$ , where  $g = 9.81$  m s<sup>-2</sup> is the acceleration due to gravity and  $\mu \sim \mathcal{O}(10^{-3})$ . Specifically, we are interested in wave disturbances of characteristic length scales that are comparable to the water depth  $h$ . Thus, the acoustic and gravity time scales become  $\tau_a \sim h/c$  and  $\tau_g \sim (h/g)^{1/2}$ , respectively. Therefore, the ratio between the two time scales is characterised by  $\tau_a/\tau_g \sim \mu^{1/2}$ .

The mathematical problem is formulated in a two-dimensional Cartesian frame of reference, with  $x$  denoting the horizontal coordinate and  $z$  the vertical coordinate. The velocity, pressure, density and free-surface-elevation fields are given by  $\mathbf{u} = u(x, z, t)\hat{\mathbf{x}} + w(x, z, t)\hat{\mathbf{z}}$ ,  $p = p(x, z, t)$ ,  $\rho = \rho(x, z, t)$  and  $\eta = \eta(x, t)$ .

The governing equations are the compressible Euler equations, expressing conservation of momentum and conservation of mass, respectively:

$$\partial_t \mathbf{u} + (\mathbf{u} \cdot \nabla) \mathbf{u} + \frac{c^2}{\rho} \nabla \rho + g \hat{\mathbf{z}} = 0, \quad \partial_t \rho + \mathbf{u} \cdot \nabla \rho + \rho (\nabla \cdot \mathbf{u}) = 0. \quad (2.1)$$

From the irrotationality condition the wave motion is described using a velocity potential  $\varphi(x, z, t)$ , such that  $\mathbf{u} = \nabla \varphi$ . The momentum and conservation of mass equations in (2.1), respectively, reduce to

$$\partial_t \varphi + \frac{1}{2} |\nabla \varphi|^2 + c^2 \log(\rho) + gz = 0, \quad (2.2)$$

$$\frac{1}{\rho} (\partial_t \rho + \mathbf{u} \cdot \nabla \rho) = \partial_t (\log(\rho)) + \nabla \varphi \cdot \nabla (\log(\rho)) = D_t \log(\rho) = -\Delta \varphi, \quad (2.3)$$

where  $\Delta = \partial_x^2 + \partial_z^2$  is the Laplacian operator in the two spatial dimensions and  $D_t = \partial_t + \mathbf{u} \cdot \nabla$  is the convective derivative. Applying  $D_t$  to (2.2), we get a single equation for the potential:

$$\partial_t^2 \varphi - c^2 \Delta \varphi + g \partial_z \varphi = -\partial_t |\nabla \varphi|^2 - \frac{1}{2} \nabla \varphi \cdot \nabla |\nabla \varphi|^2. \quad (2.4)$$

In order for the equation above to admit a unique solution, it has to be subject to proper boundary conditions. Since the flow is a free-surface flow, we need to impose two boundary conditions along the free surface  $z = \eta(x, t)$  which itself forms part of the unknowns. These boundary conditions are a kinematic boundary condition and a dynamic boundary condition and read, respectively,

$$\partial_t \varphi + \frac{1}{2} |\nabla \varphi|^2 + gz = 0 \quad \text{and} \quad \partial_t \eta + \partial_x \varphi \partial_x \eta = \partial_z \varphi, \quad \text{both on } z = \eta. \quad (2.5)$$

In addition, a no-penetration boundary condition holds at the bottom boundary, i.e.  $\partial_z \varphi = 0$ , at  $z = -h$ .

Employing  $h$  as the length scale and  $\tau_a$  as the time scale, the non-dimensional compressible wave equation (2.4) in the fluid interior  $(x, z) \in (-\infty, +\infty) \times (-1, 0)$  becomes (Kadri & Akylas 2016)

$$\partial_t^2 \varphi - \Delta \varphi + \mu \partial_z \varphi = -\partial_t |\nabla \varphi|^2 - \frac{1}{2} \nabla \varphi \cdot \nabla |\nabla \varphi|^2. \quad (2.6)$$

Perturbing about  $\eta = 0$ , conditions (2.5) become (Benney (1962))

$$\begin{aligned} \partial_t^2 \varphi + \mu \partial_z \varphi = & -\partial_t |\nabla \varphi|^2 + \frac{1}{\mu} \partial_t \left( \partial_t \varphi \partial_{tz}^2 \varphi \right) - \partial_x \varphi \partial_{xt}^2 \varphi + \partial_z^2 \varphi \partial_t \varphi \\ & + \frac{1}{2\mu} \partial_{tz}^2 \left( \partial_t \varphi |\nabla \varphi|^2 \right) - \frac{1}{2} \partial_x \varphi \partial_x |\nabla \varphi|^2 + \frac{1}{2} \partial_z^2 \varphi |\nabla \varphi|^2 - \frac{1}{\mu^2} \partial_t \left( \partial_t \varphi (\partial_{tz}^2 \varphi)^2 \right) \\ & - \frac{1}{2\mu^2} \partial_t \left( \partial_{tzz}^3 \varphi (\partial_t \varphi)^2 \right) + \frac{1}{\mu} \partial_x \varphi \partial_x \left( \partial_t \varphi \partial_{tz}^2 \varphi \right) + \frac{1}{\mu} \partial_t \varphi \partial_{tx}^2 \varphi \partial_{xz}^2 \varphi \\ & - \frac{1}{\mu} \partial_t \varphi \partial_z^2 \varphi \partial_{tz}^2 \varphi - \frac{1}{2\mu} \partial_z^3 \varphi (\partial_t \varphi)^2, \quad \text{on } z = 0. \end{aligned} \tag{2.7}$$

Equation (2.7) is the cubic truncation of the fully nonlinear free-surface boundary condition expressed in terms of the velocity potential only. Thus, the wave amplitudes need to be sufficiently small so that the remainder is negligible relative to the terms in (2.7).

Finally, the bottom boundary condition is

$$\partial_z \varphi = 0, \quad \text{on } z = -1. \tag{2.8}$$

Unlike the deep-water case studied by Kadri & Akylas (2016), here in the limit  $\mu \ll 1$  (2.6) pertains to water compressibility which reflects its importance on gravity waves for the specific choice of the length scale  $h$ .

### 3. Linear solution

Neglecting the nonlinear terms in (2.6) and (2.7), we look for a solution in terms of travelling waves in the  $x$ -direction with amplitudes modulated in  $z$ , namely

$$\varphi(x, z, t) = \sum_{n=1}^{\infty} A_n f_n(z) e^{i(k_n x - \omega_n t)} + \text{c.c.}, \tag{3.1}$$

where c.c. stands for complex conjugate, and the mode number  $n$  is omitted in the following, for brevity, unless necessary. Substituting (3.1) into (2.6)–(2.8) yields a generalised eigenvalue problem for the unknowns modes  $f_n(z)$  of the form

$$\begin{aligned} f'' - \mu f' + (\omega^2 - k^2) f &= 0 \quad (-1 < z < 0), \\ \mu f' - \omega^2 f &= 0 \quad (z = 0), \\ f' &= 0 \quad (z = -1). \end{aligned} \tag{3.2}$$

Equations (3.2) are solved asymptotically for  $\mu \ll 1$ .

#### 3.1. Linear gravity modes

To examine the effects of gravity we rescale the frequency as  $\omega \rightarrow \mu^{1/2} \omega$  and take the limit  $\mu = 0$  of system (3.2), obtaining the eigensolutions

$$f(z) = \cosh k(z + 1) + \mathcal{O}(\mu), \quad k > 0, \tag{3.3}$$

with dispersion relation

$$\omega^2 = k \tanh k + \mathcal{O}(\mu). \tag{3.4}$$

3.2. *Linear acoustic modes*

For the acoustic modes, the leading order in (3.2) yields

$$f(z) = \sin \lambda z + \mathcal{O}(\mu), \tag{3.5}$$

where

$$\omega^2 = k^2 + \lambda^2 + \mathcal{O}(\mu) \quad \text{and} \quad \lambda^{(n)} = (n + 1/2)\pi, \quad n = 0, 1, 2, \dots, \tag{3.6}$$

where superscript  $(n)$  indicates the eigenvalue mode number, which is omitted for brevity.

3.3. *Resonant triads*

Consider a triad comprising two acoustic modes characterised by wavenumbers  $(k_1, k_2)$  and frequencies  $(\omega_1, \omega_2)$ , satisfying the dispersion relation (3.6) and a gravity mode with wavenumber  $k_3$  and frequency  $\mu^{1/2}\omega_3$ , with  $\omega_3$  observing the gravity dispersion relation (3.4). Resonant interaction among the triad is possible if the following resonance conditions are met:

$$k_1 + k_2 = k_3, \quad \omega_1 + \omega_2 = \mu^{1/2}\omega_3. \tag{3.7}$$

Note that numerically  $\omega_2$  in (3.7) must have an opposite sign compared with  $\omega_1$ , and the current convention is employed for convenience. In order for resonant triad interaction to occur, (3.7), together with the dispersion relations for the gravity and acoustic modes, must be satisfied.

For the triad resonance to be satisfied there are two scenarios. The first scenario comprises two acoustic modes of almost identical wavenumbers and frequencies, and thus we can write

$$|k_1| + |k_2| = k, \quad |\omega_1| - |\omega_2| = \Omega, \tag{3.8}$$

where  $|k_1| = (k + \mu^{1/2})/2$ ,  $|k_2| = (k - \mu^{1/2})/2$  and  $\Omega$  is the gravity-mode frequency which must be  $\sim \mathcal{O}(\mu^{1/2})$ . Under this setting, we can approximate the frequencies in the form

$$|\omega_j| \simeq |k_j|/2 + \lambda_j^2/(2|k_j|), \quad j = 1, 2, \tag{3.9}$$

which requires

$$\Omega \sim \mu^{1/2} + (\lambda_1^2 - \lambda_2^2)/k. \tag{3.10}$$

Therefore, for (3.8) to be satisfied the interaction must comprise the same acoustic mode numbers  $n$ , i.e.  $\lambda_1 = \lambda_2$ , and thus the second term of the right-hand side of (3.10) must be zero.

The second scenario requires the conditions

$$|k_1| - |k_2| = |k_3|, \quad |\omega_1| - |\omega_2| = \mu^{1/2}|\omega_3|. \tag{3.11}$$

Under this setting, making use of (3.9) and after some algebra we arrive at the condition

$$|k_3|^2 = \frac{|k_1|\lambda_2^2 - |k_2|\lambda_1^2}{|k_1k_2|}. \tag{3.12}$$

Condition (3.12) indicates that interaction between acoustic modes with different  $n$  is possible. In the case that  $\lambda_1 = \lambda_2 \equiv \lambda$ , the condition reduces to  $|k_1k_2k_3| = \lambda^2$ .

#### 4. Amplitude equations

In this section we derive the amplitude evolution equations of the triad discussed in the previous section. Specifically, we apply the method of multiple scales as employed by Kadri & Akylas (2016). Initially, we derive the amplitude equations with no spatial modulation, hence assuming that the amplitude of each mode is a function of a slow temporal variable  $T = \mu t$ .

Building on the scaling arguments presented above, the velocity potential for the triad is expressed as follows:

$$\begin{aligned} \varphi = & \epsilon \left[ A_1(T) \sin(\lambda_1 z) e^{i\theta_1} + \text{c.c.} \right] + \epsilon \left[ A_2(T) \sin(\lambda_2 z) e^{i\theta_2} + \text{c.c.} \right] \\ & + \alpha \left[ S(T) \cosh k_3(z + 1) e^{i\theta_3} + \text{c.c.} \right] + \dots \end{aligned} \quad (4.1)$$

where  $\theta_j = k_j x - \omega_j t$ , with  $j = \{1, 2\}$ ,  $\theta_3 = k_3 x - \mu^{1/2} \omega_3 t$  and  $\epsilon$  and  $\alpha$  are coefficients depending on  $\mu$ . Their dependence is specified in the next section.

##### 4.1. Interaction time scale

To estimate the appropriate interaction time scale, we note that the identified triads consist of two acoustic modes and a gravity wave. Let the velocity potential of each acoustic mode be  $\mathcal{O}(\epsilon)$ , where  $0 < \epsilon \ll 1$ . The nonlinear interaction between these acoustic modes, governed by the quadratic terms in (2.6), (2.7) and (2.8), excites the gravity wave, whose velocity potential grows to  $\mathcal{O}(\alpha)$ , where  $\alpha$  will be specified later. Based on previous analyses of triad interactions (e.g. Bretherton 1964), this energy transfer is expected to occur on a time scale of  $\mathcal{O}(\alpha/\epsilon^2)$ .

Next, consider the interaction between the  $\mathcal{O}(\alpha)$  gravity wave and one of the  $\mathcal{O}(\epsilon)$  acoustic modes. Accounting for the fact that the velocity field of the gravity wave is  $\mathcal{O}(\alpha/\mu^{1/2})$ , as indicated in (3.7), the time scale for energy flow to the other acoustic mode is expected to be  $\mathcal{O}(\mu^{1/2}/\alpha)$ .

For a fully coupled three-wave interaction resulting in an equitable energy distribution among all triad members, these two separate interactions must occur on the same time scale. This condition requires

$$\alpha = \epsilon \mu^{1/4}. \quad (4.2)$$

Now it becomes clear that cubic self-interaction of acoustic modes must take a much longer time scale. Therefore, cubic terms can be neglected in the derivation of the amplitude equations.

##### 4.2. Acoustic modes

We introduce a small-order correction term to the background potential (4.1) in the form  $G_j(z, T) e^{i\theta_j}$ . Substituting this into (2.6), (2.7) and (2.8), and isolating the resonant acoustic terms, we obtain the following equations for  $G_j$ :

$$\partial_z^2 G_j + \lambda_j^2 G_j = -2\epsilon \mu i \omega_j \sin(\lambda_j z) \dot{A}_j + \epsilon \mu \lambda_j \cos(\lambda_j z) A_j \quad (-1 < z < 0), \quad (4.3a)$$

$$G_j = \epsilon \mu \frac{\lambda_j}{\omega_j^2} A_j + \mu^{-1/4} \epsilon^2 i \frac{\omega_j \omega_3}{\omega_i} \lambda_j \cosh(k_3) A_i^* S \quad (z = 0), \quad (4.3b)$$

$$\partial_z G_j = 0 \quad (z = -1), \quad (4.3c)$$

where the over dot stands for time derivative. Application of the Fredholm alternative as a solvability condition returns an amplitude equation of the form

$$\mu^{5/4} \dot{A}_j = \mu^{5/4} \frac{i}{\omega_j} \left( \frac{1}{2} - \frac{\lambda_j^2}{\omega_j^2} \right) A_j + \epsilon \lambda_i \lambda_j \cosh(k_3) \frac{\omega_i \omega_3}{\omega_j^2} A_i^* S. \quad (4.4)$$

In order to balance all terms in (4.4), we require that  $\epsilon = \mu^{5/4}$ , so the final form of the amplitude equations for the two acoustic modes reads

$$\dot{A}_j = \frac{i}{\omega_j} \left( \frac{1}{2} - \frac{\lambda_j^2}{\omega_j^2} \right) A_j + \lambda_i \lambda_j \cosh(k_3) \frac{\omega_i \omega_3}{\omega_j^2} A_i^* S. \quad (4.5)$$

### 4.3. Gravity mode

Similarly to the approach taken previously for the acoustic perturbations, we introduce a correction term for the gravity contribution in the form  $G_3(z, T)e^{i\theta_3}$ . Substituting this into the field (2.6) and the boundary conditions (2.7)–(2.8), we derive the following system:

$$k_3^2 G_3 - \partial_z^2 G_3 = 0 \quad (-1 < z < 0), \quad (4.6a)$$

$$\partial_z G_3 = \omega_3^2 G_3 + 2i\omega_3 \cosh(k_3) \dot{A}_3 + 2i\lambda_i \lambda_j A_i A_j \quad (z = 0), \quad (4.6b)$$

$$\partial_z G_3 = 0 \quad (z = -1). \quad (4.6c)$$

Applying the solvability condition, we obtain the amplitude equation for  $S(T)$ :

$$\dot{S} = -\frac{\lambda_1 \lambda_2}{\cosh(k_3)} A_1 A_2. \quad (4.7)$$

### 4.4. Spatial modulation

When spatial modulation is allowed, a slowly varying spatial coordinate  $X = \mu x$  has to be introduced, leading to the appearance of a term of the form  $2\epsilon \mu i k_j \sin(\lambda_j z) \partial_X A_j$  on the right-hand side of equation (4.3a). The solvability condition then yields a generalised set of amplitude equations incorporating spatial dependence:

$$\partial_T A_1 + \frac{k_1}{\omega_1} \partial_X A_1 = \frac{i}{\omega_1} \left( \frac{1}{2} - \frac{\lambda_1^2}{\omega_1^2} \right) A_1 + \lambda_1 \lambda_2 \cosh(k_3) \frac{\omega_2 \omega_3}{\omega_1^2} A_2^* S, \quad (4.8a)$$

$$\partial_T A_2 + \frac{k_2}{\omega_2} \partial_X A_2 = \frac{i}{\omega_2} \left( \frac{1}{2} - \frac{\lambda_2^2}{\omega_2^2} \right) A_2 + \lambda_1 \lambda_2 \cosh(k_3) \frac{\omega_1 \omega_3}{\omega_2^2} A_1^* S, \quad (4.8b)$$

$$\partial_T S = -\lambda_1 \lambda_2 \operatorname{sech}(k_3) A_1 A_2, \quad (4.8c)$$

where  $k_j/\omega_j$ , with  $j = 1, 2$ , represent the group velocities of the two acoustic modes. It is worth noting that the equation for  $S$  remains unchanged compared with the case without spatial dependence. This is because spatial variations for gravity modes occur on a much larger spatial scale than those for the acoustic modes.

**5. Energy considerations: non-spatial equations**

In this section, we aim to provide deeper insights into (4.5) and (4.7) and their solutions. We begin by reducing the system to a single ordinary differential equation, enabling us to construct the phase portrait of the corresponding dynamical system. Subsequently, we present analytical results derived under suitable approximations and compare them with numerical simulations. Thus, we can write

$$\dot{A}_1 = i\beta_1 A_1 + \alpha_1 A_2^* S, \tag{5.1a}$$

$$\dot{A}_2 = i\beta_2 A_2 + \alpha_2 A_1^* S, \tag{5.1b}$$

$$\dot{S} = -\alpha_3 A_1 A_2, \tag{5.1c}$$

where

$$\alpha_1 = \lambda_1 \lambda_2 \cosh(k_3) \frac{\omega_2 \omega_3}{\omega_1^2}, \quad \alpha_2 = \lambda_1 \lambda_2 \cosh(k_3) \frac{\omega_1 \omega_3}{\omega_2^2}, \quad \alpha_3 = \frac{\lambda_1 \lambda_2}{\cosh(k_3)}, \tag{5.2}$$

$$\beta_1 = \frac{1}{\omega_1} \left( \frac{1}{2} - \frac{\lambda_1^2}{\omega_1^2} \right), \quad \beta_2 = \frac{1}{\omega_2} \left( \frac{1}{2} - \frac{\lambda_2^2}{\omega_2^2} \right).$$

Multiplying the terms in (5.1) by their associated amplitude’s complex conjugate, and adding the product of the amplitudes with the complex conjugate of the terms, results in

$$\begin{aligned} \frac{d|A_1|^2}{dT} &= \alpha_1 A_1 A_2 S^* + \alpha_1 A_1^* A_2^* S, \\ \frac{d|A_2|^2}{dT} &= \alpha_2 A_1 A_2 S^* + \alpha_2 A_1^* A_2^* S, \\ \frac{d|S|^2}{dT} &= -\alpha_3 A_1 A_2 S^* - \alpha_3 A_1^* A_2^* S. \end{aligned} \tag{5.3}$$

Through straightforward algebra, the following invariants (constants of motion) can be derived from (5.3):

$$\begin{aligned} E_0 &\equiv \alpha_1 \alpha_2 |S|^2 + \frac{\alpha_3 \alpha_2}{2} |A_1|^2 + \frac{\alpha_3 \alpha_1}{2} |A_2|^2, \\ I_0 &\equiv \left( \alpha_2 |A_1|^2 - \alpha_1 |A_2|^2 \right), \quad I_j \equiv \left( \alpha_3 |A_j|^2 + \alpha_j |S|^2 \right), \quad j = 1, 2, \end{aligned} \tag{5.4}$$

$$Q \equiv |A_1| |A_2| |S| \sin(\arg S - \arg A_1 - \arg A_2) + (\beta_1 / \alpha_1) |A_1|^2 + (\beta_2 / \alpha_2) |A_2|^2,$$

where  $E_0$  represents the initial energy of the system (Craig 1988),  $I_j$  for  $j = 0, 1, 2$  are the Manley–Rowe relations (Manley & Rowe 1956) and  $Q$  is a Hamiltonian of the system (Martin & Segur 2016, pp. 74–75).

The conservation of energy equation is useful for reducing system (5.1) to a single ordinary differential equation for the gravity-wave amplitude  $S$ . By differentiating (5.1c) with respect to time and utilising (5.1a), (5.1b) alongside (5.4), we obtain

$$\ddot{S} = -i(\beta_1 + \beta_2)\dot{S} - 2S \left( E_0 - \alpha_1 \alpha_2 |S|^2 \right). \tag{5.5}$$

We solve equation (5.5) with the initial conditions  $S(0) = 0.5$  and  $\dot{S}(0) = 0$ . The solutions exhibit periodic behaviour, as shown in figure 1, across different resonant triads (distinguished by varying  $k_3$ ) and for two sets of acoustic axial mode numbers:  $n = (0, 0)$ ,

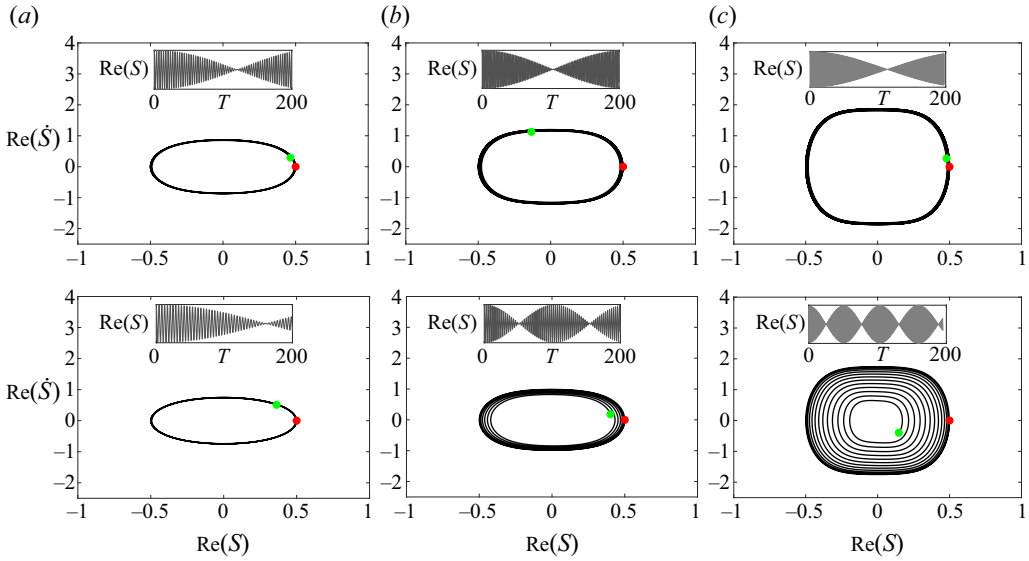


Figure 1. Phase portraits for  $n = (0, 0)$  (top panels) and  $n = (0, 1)$  (bottom panels) for initial conditions  $S(0) = 0.5, \dot{S}(0) = 0$ : (a)  $k_3 = 1$ ; (b)  $k_3 = 1.5$ ; (c)  $k_3 = 2$ . Red dot indicates the starting point ( $T = 0$ ); green dot the end point ( $T = 20$ ) in the phase portrait. For each case, the periodic time behaviour is shown above the phase portraits over an extended time frame  $T = 200$ .

i.e.  $\lambda_1 = \lambda_2 = \pi/2$  in the upper panels, and  $n = (0, 1)$ , i.e.  $(\lambda_1, \lambda_2) = (\pi/2, 3\pi/2)$  in the lower panels. Following Craik (1988, pp. 129–130) and Martin & Segur (2016), it can be shown that the solutions in figure 1 exhibit a non-explosive periodic behaviour (see Appendix A).

Notably, for the case  $n = (0, 1)$ , the last two panels highlight a pronounced decrease followed by an increase in the amplitude of  $S$  within the considered time range. This rapid variation in the gravity-wave amplitude is largely absent in the other panels, where the system’s orbits remain consistent.

Analytical solutions to (5.5) can be derived in closed form, particularly when  $\beta_1 + \beta_2 \ll 1$ . Under this condition, the imaginary term in (5.5) vanishes, allowing  $S(T)$  to be treated as a purely real function. It satisfies a Duffing-type equation:

$$\ddot{S} + 2E_0S - 2\alpha_1\alpha_2S^3 = 0, \tag{5.6}$$

with initial conditions  $S(0) = 1/2; \dot{S}(0) = 0$ . Following Salas & Castillo (2014), this differential problem (5.6) admits the closed-form solution

$$S(T) = \frac{1}{2} \text{cn} \left[ \left( 2E_0 - \frac{\alpha_1\alpha_2}{2} \right)^{1/2} t, \left( \frac{-\alpha_1\alpha_2}{8E_0 - 4\alpha_1\alpha_2} \right)^{1/2} \right], \tag{5.7}$$

where  $\text{cn}[\cdot]$  denotes the elliptic Jacobi function (Abramowitz & Stegun 1965). A comparison between numerical and analytical solutions (5.7) reveals that the system exhibits a periodic trend, with good agreement between the two approaches for smaller values of  $k_3$  (figure 2). As  $k_3$  increases, differences in the phase of the oscillations become apparent, due to the deviation of  $\beta_1 + \beta_2$  from zero. This leads to a growing discrepancy between the analytical and numerical solutions. However, for relatively small values of  $k_3$ , the deviation between the analytical and the numerical solutions becomes small.

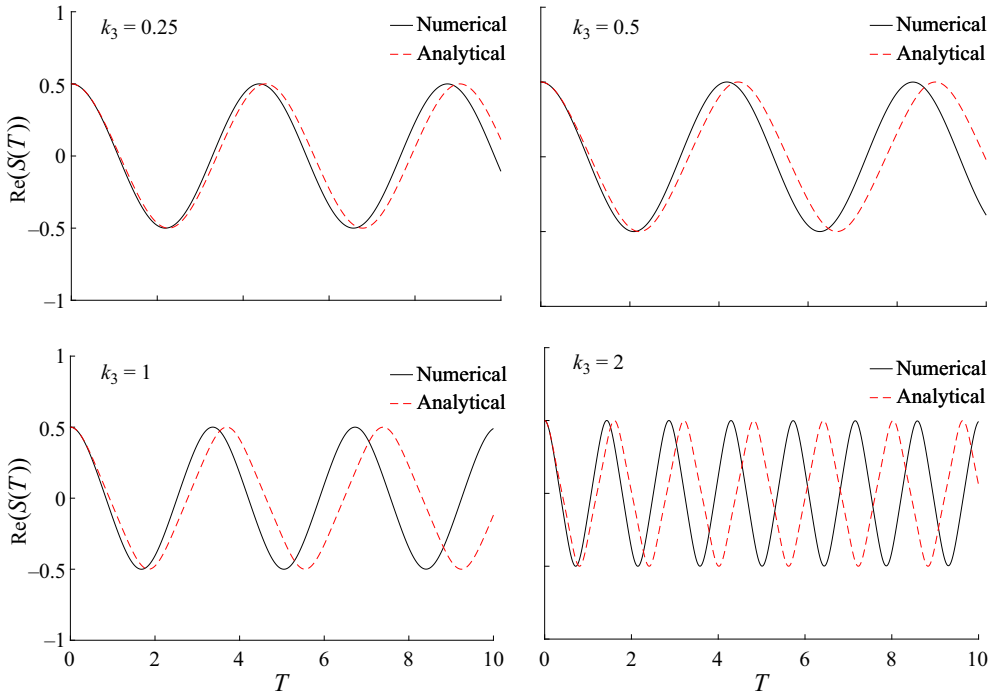


Figure 2. Numerical and analytical solutions (5.7) for  $n = (0, 0)$ .

### 6. Results and discussion

To analyse the effects of spatial variations on the nonlinear dynamics of the system we solve the amplitude equations (4.8) numerically with a set of acoustic modes with  $n = \{(0, 0), (0, 1), (1, 1)\}$ . The numerical scheme adopted is the method of lines with upwind finite differentiation of spatial derivatives (Schuesser & Griffiths 2009). The boundary conditions are of non-reflecting type and the location where these must be imposed depends on the sign of the group velocities of each acoustic mode, which for the cases we are showing is taken to be negative for the first mode and positive for the second mode (unless explicitly stated). Thus, as the first acoustic mode propagates to the left, the boundary condition must be imposed on the right-end point. On the contrary, as the second acoustic wave propagates to the right, the boundary condition must be imposed on the left-end point.

In the computations reported below we take the initial values

$$S(\xi, 0) = e^{-\xi^2}, \quad A_j(\xi, 0) = Ae^{-\xi^2/\sigma^2}, \quad j = 1, 2, \quad (6.1)$$

where  $\sigma$  is a measure of the acoustic wave packet width. A parametric study is carried out by varying the initial amplitude of the acoustic modes  $A$ , the resonant gravity wavenumber  $k_3$  and  $\sigma$ . In particular,  $(k_3, A, \sigma)$  span in  $[0.2, 3] \times [0.05, 1] \times [0.1, 10]$ . This allows one to cover both intermediate finite-depth and deep-water gravity waves with acoustic modes having either small magnitude or the same order of magnitude as the gravity wave. The motivation is to find a set of parameters that either minimises or maximises the amplitude of the gravity wave with respect to its initial value. For this purpose, we define a ‘difference

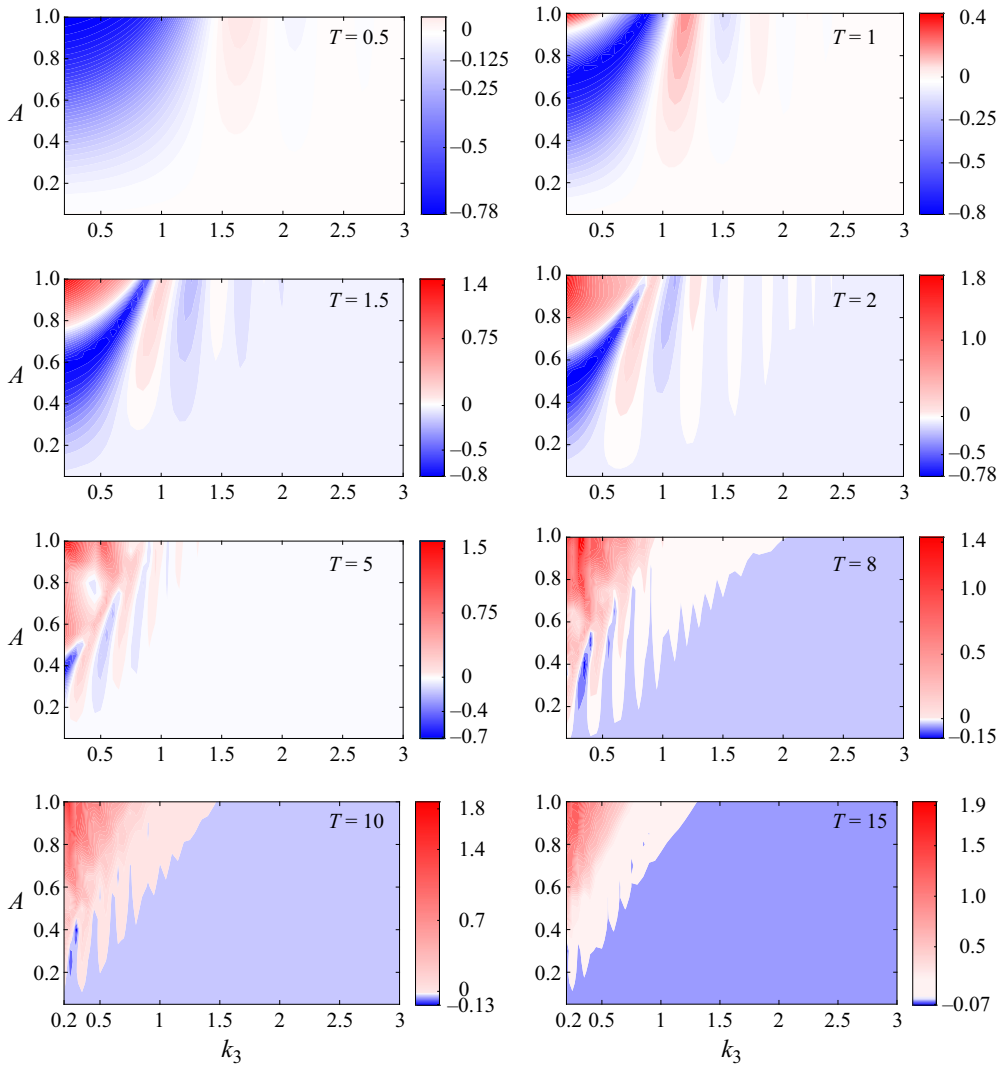


Figure 3. Difference function  $D_S$  (equation (6.2)) for  $\sigma = 1$ ,  $n = (0, 0)$  and several times  $T$ .

function'  $D_S = D_S(T, A, \sigma, k_3)$  which measures the reduction or the amplification of the gravity-wave amplitude as

$$D_S = \max_{\xi} (|S(\xi; T)| - 1). \quad (6.2)$$

Figure 3 presents contours of the difference function computed for  $\sigma = 1$  at various times  $T = 0.5 \dots 15$ . The largest decay rate of the gravity-wave amplitude occurs within times of at most order one. For  $T \geq 5$ , the amplification rate surpasses the corresponding decay rate, although certain bands in the  $k_3$ - $A$  plane, particularly for small wavenumbers and acoustic initial amplitudes, still exhibit decay. Specific configurations of the acoustic wave packet width  $\sigma$  and amplitude  $A$  may have a significant effect on the decay rate, as shown in figure 4. In particular, small values of  $\sigma$  produce bands where the difference function is negative, corroborating the trends observed in figure 3. However, for smaller

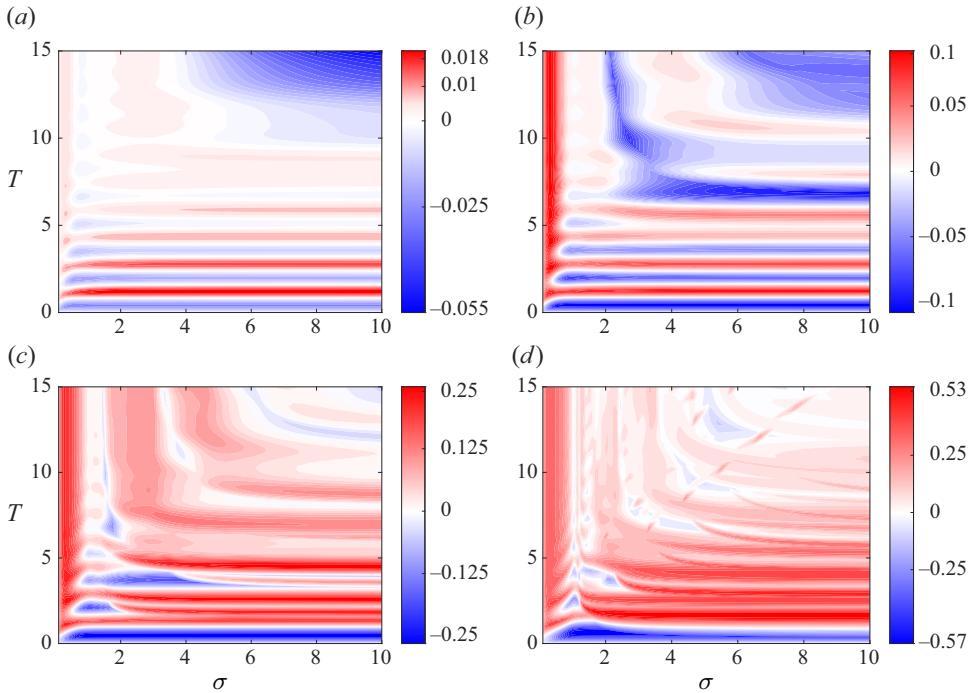


Figure 4. Difference function  $D_S$  as a function of slow time scale  $T$ , acoustic width  $\sigma$ , mode numbers  $n = (0, 0)$ , resonant gravity wavenumber  $k_3 = 1$  and different initial acoustic amplitudes: (a)  $A = 0.25$ ; (b)  $A = 0.5$ ; (c)  $A = 0.75$ ; (d)  $A = 1$ .

amplitudes,  $A = 0.25$  and  $A = 0.5$ , larger  $\sigma$  leads to wider regions of decreasing gravity-wave amplitude, at larger time  $T$ . This observation is confirmed, when considering configurations with  $\sigma = 10$ , as shown in figure 5. In this case, reductions in gravity-wave amplitude are generally less significant than in the previous scenario, except within specific bands in the  $k_3$ – $A$  plane at certain times.

The interaction involving  $n = (0, 1)$  and  $(1, 1)$  results in more periodic behaviour, as expected from higher modes (see figure 6). For higher modes, a steady state is typically reached more quickly, after which the amplified gravity-wave amplitude remains constant. However, it appears that a suitable combination of  $(\sigma, A)$  can always be found to control the type of resonance, resulting in either amplification or reduction of the initial gravity-wave peak (see the bottom-right panel of figure 6).

Lastly, we considered the case where only a single mode is initially sent against the gravity mode. However, this scenario proved less effective for reducing the amplitude of gravity waves. In practice, the difference function (6.2) does not exhibit negative contours, meaning that the amplitude of the initial surface gravity wave is either amplified or, at best, remains unchanged (see Appendix B).

## 7. Concluding remarks

Motivated by the work of Kadri (2016, 2017), we studied the nonlinear interaction between two acoustic modes and a single gravity wave in water of finite constant depth, focusing on energy exchange facilitated by resonant triad interactions. The derivation of amplitude equations using the method of multiple scales highlighted the dominant role of quadratic

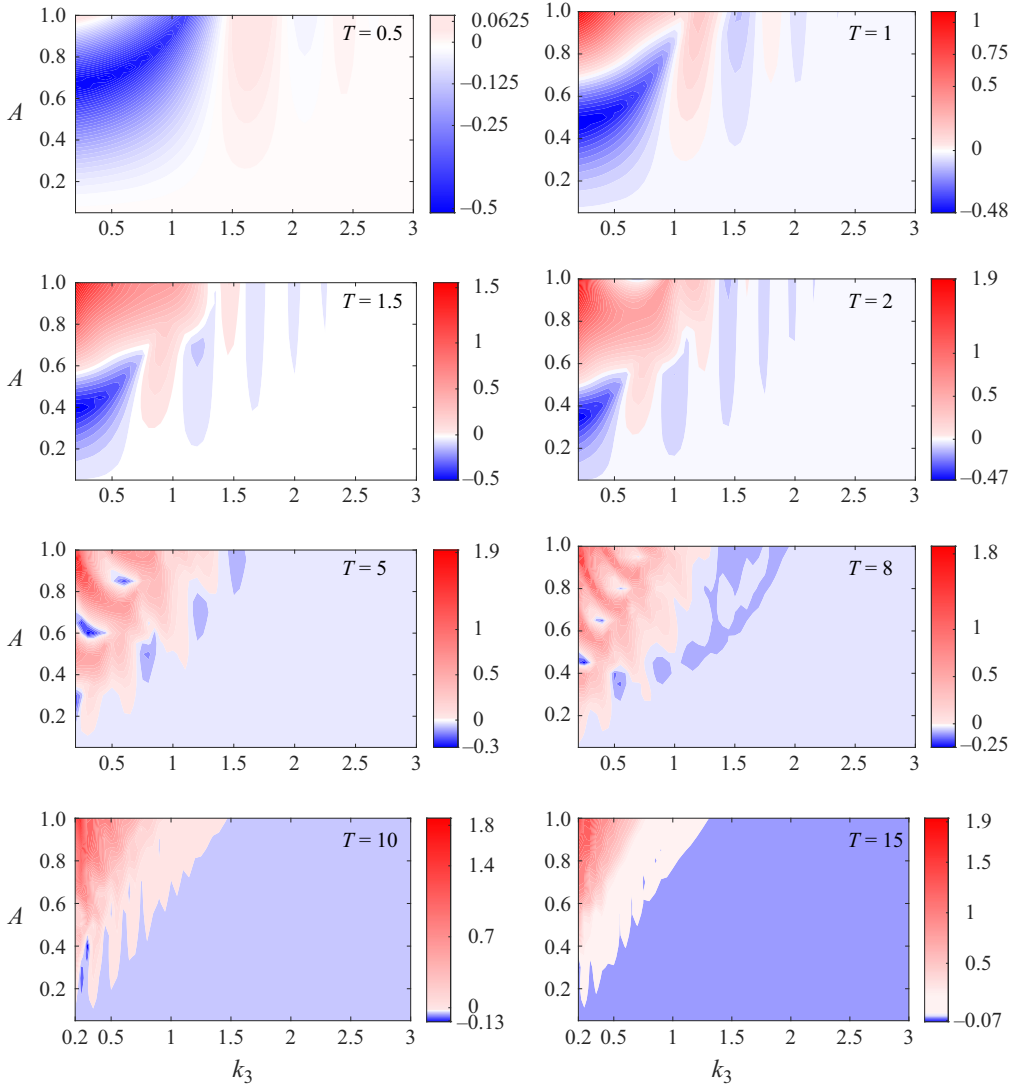


Figure 5. Difference function  $D_S$  for  $\sigma = 10$ ,  $n = (0, 0)$  and several times  $T$ .

nonlinearities, while cubic terms were found to be negligible on the time scales considered, unlike the case of two gravity waves and a single acoustic mode studied by Kadri & Akylas (2016). Notably, the amplitude equations emerge under a non-standard scaling due to the intrinsic time difference scales involved in the propagation of linear gravity and acoustic waves, separately.

The efficiency of energy transfer was shown to depend strongly on water depth. In deeper water, the energy transfer to the gravity mode is minimal, whereas in shallower regimes, the interaction becomes more significant. Numerical simulations revealed that the resonant gravity-wave amplitude could be either amplified or reduced, depending on the initial parameters, such as the gravity wavenumber, acoustic amplitude and wave packet width.

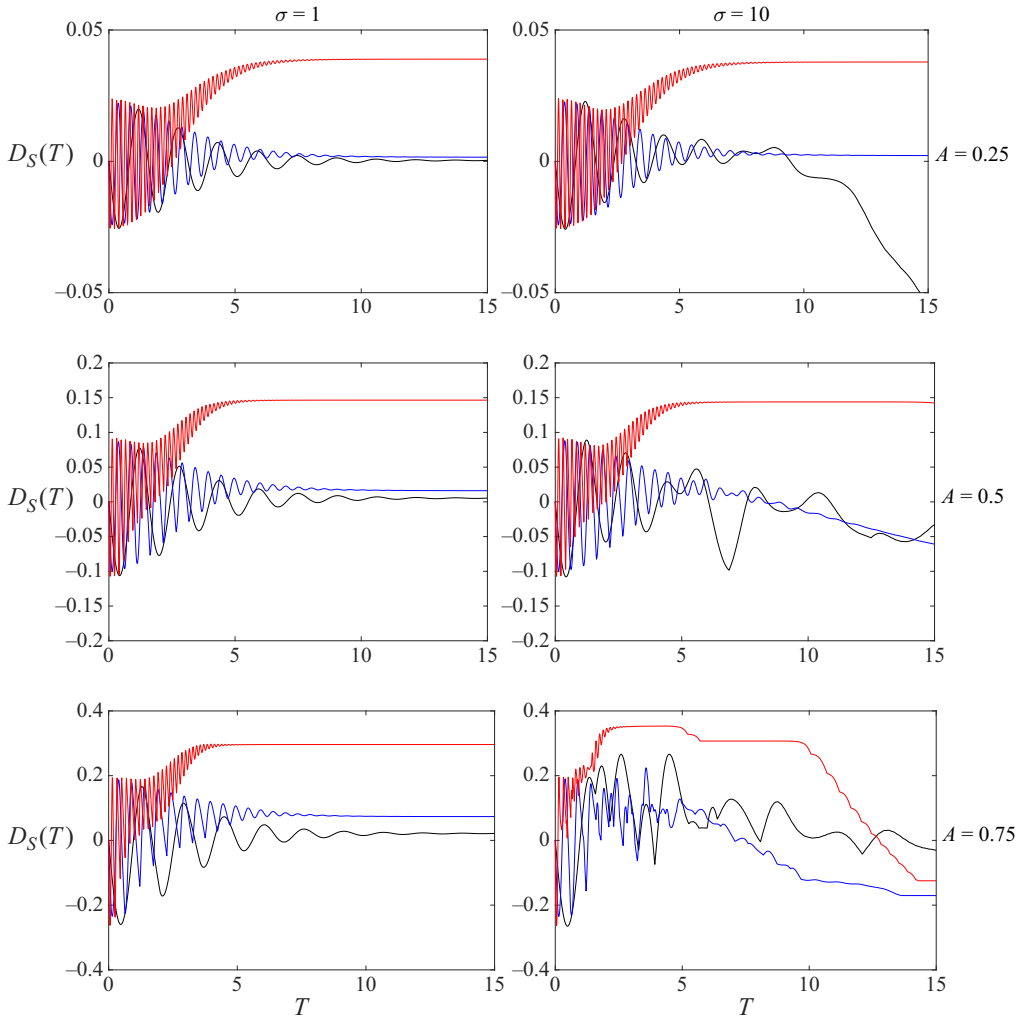


Figure 6. Difference function  $D_S$  as a function of slow time scale  $T$ , with  $k_3 = 1$  and acoustic amplitudes  $A = 0.25$  (top panels),  $A = 0.5$  (middle panels),  $A = 0.75$  (bottom panels); and  $\sigma = 1$  (left-hand panels) and  $\sigma = 10$  (right-hand panels). Black:  $n = (0, 0)$ . Blue:  $n = (0, 1)$ . Red:  $n = (1, 1)$ .

Two key findings emerged from the scenario where all three waves have non-zero initial amplitudes. First, the reduction in gravity-wave amplitude is most significant for low resonant gravity wavenumbers and initial acoustic amplitudes of order one. Second, the timing of this reduction depends on the initial width of the acoustic wave packet, with more localised acoustic modes leading to earlier reductions. In contrast, when a single acoustic mode initially interacts with a gravity wave, the interaction generates a second acoustic mode which feeds the gravity wave as well, resulting in the latter maintaining its initial amplitude or experiencing further growth, as shown in [figure 8](#). This highlights the limited effectiveness of single-mode interactions in mitigating gravity-wave amplitudes, which is in agreement with [Kadri \(2016\)](#).

These findings have potential implications for tsunami mitigation using triad resonance ([Kadri 2017](#)), where reducing gravity-wave amplitudes could significantly decrease the

impact of tsunamis. In principle, resonant interactions could be timed such that maximum amplitude reduction is achieved as the tsunami approaches the shoreline. Although acoustic modes may generate additional gravity waves, the tsunami energy would be redistributed over a broader area, thereby minimising its impact at the shoreline. However, implementing this approach requires generating acoustic waves on a scale beyond current technological capabilities. Moreover, finely tuning the resonant triad would necessitate real-time, detailed knowledge of tsunami characteristics, which presents a significant technical challenge. Additionally, the mitigation of large tsunamis requires further study, particularly in the shallow-water regime. In this context, seabed elasticity plays an essential role (Eyov *et al.* 2013; Williams & Kadri 2023), enabling the propagation of leading acoustic modes at nearly twice the speed of sound in water due to coupling with the elastic seabed layer, resulting in the formation of Scholte waves. Understanding these dynamics is an ongoing area of research.

Another implication may find application in improving energy harnessing of surface gravity waves in deeper water. Surface gravity waves in deep water present a significant opportunity for renewable energy harnessing, as they can propagate energy over long distances with minimal loss. Winds generate wave energy at a global rate of approximately  $5.6 \times 10^{13}$  W, comparable to the world's current power consumption of  $1.5 \times 10^{13}$  W (Rascle *et al.* 2008; Rascle & Ardhuin 2013). While the exact fraction of this energy that is practically exploitable remains uncertain due to the nascent state of wave-energy technology, its potential is vast (Cruz 2007; Multon 2013). Sending a single acoustic mode that resonates with the gravity wave within the triad mechanism can significantly amplify the gravity wave's amplitude, as shown in figure 8, particularly for smaller  $k_3$  (i.e. shallower water). Nevertheless, the amplitude amplification process requires input energy, part of which would be dissipated unless a mechanism is developed to also capture and utilise the acoustic energy (Tian & Kadri 2018). Exploring such mechanisms remains a subject for future research.

It is worth noting that restoring the physical dimensions, the maximum acoustic pressure would scale as  $p_0 \sim 2\mu^{5/4}|\omega_j|A\rho c^2$ . In the examples shown in this study  $p_0 \sim \mathcal{O}(10^5)$  Pa, which is achieved for  $\mathcal{O}(1)$  frequencies and amplitudes. If the dynamic pressure were to approach  $\mathcal{O}(10^7)$  Pa, which characterises the hydroacoustic pressure at the bottom of the ocean, then cavitation effects would, in principle, need to be considered. However, in such a regime, the triad interaction mechanism described in this study would no longer hold, as the underlying assumptions of the model would break down.

**Supplementary movies.** Supplementary movies are available at <https://doi.org/10.1017/jfm.2025.111>.

**Acknowledgements.** This work was funded by Leverhulme Trust Research Project grant number 523930.

**Declaration of interests.** The authors report no conflict of interest.

**Data availability statement.** The data that support the findings of this study are available from the corresponding author upon reasonable request.

## Appendix A

Let us define the wave actions of the three modes:

$$\mathcal{L}_{A_1} = \frac{\alpha_2\alpha_3}{2\omega_1}|A_1|^2, \quad \mathcal{L}_{A_2} = \frac{\alpha_1\alpha_3}{2\omega_2}|A_2|^2, \quad \mathcal{L}_S = \frac{\alpha_1\alpha_2}{\omega_3}|S|^2. \quad (\text{A1})$$

Following Craik (1988, pp. 129–130) and Martin & Segur (2016), the periodicity of the solutions is ensured as the signs of the coefficients ( $\alpha_1$ ,  $\alpha_2$ ,  $\alpha_3$ ) and the wave actions

	$n$	$\alpha_1$	$\alpha_2$	$\alpha_3$	$\mathcal{L}_{A_1}$	$\mathcal{L}_{A_2}$	$\mathcal{L}_S$
(a)	(0, 0)	2.06	-1.96	1.59	(-)	(+)	(-)
	(0, 1)	0.97	-0.97	4.79	(-)	(+)	(-)
(b)	(0, 0)	4.01	-3.76	1.04	(-)	(+)	(-)
	(0, 1)	2.78	-2.74	3.14	(-)	(+)	(-)
(c)	(0, 0)	7.17	-6.68	0.65	(-)	(+)	(-)
	(0, 1)	6.47	-6.33	1.96	(-)	(+)	(-)

Table 1. Coefficients ( $\alpha_1, \alpha_2, \alpha_3$ ) and signs of the wave actions ( $\mathcal{L}_{A_1}, \mathcal{L}_{A_2}, \mathcal{L}_S$ ) for cases (a), (b) and (c) shown in figure 1.

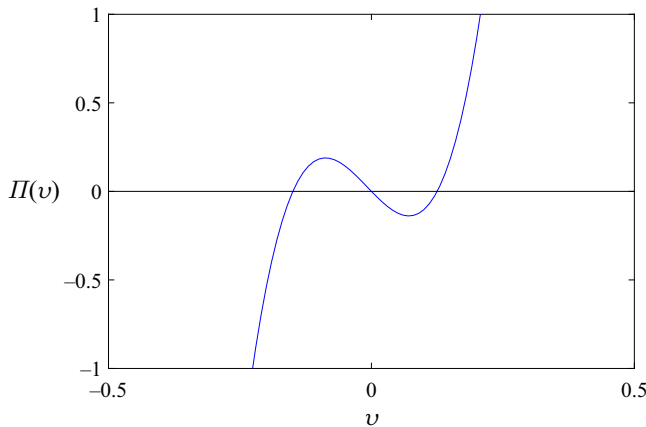


Figure 7. Graphical representation of the potential (B3) for the solution with parameters  $n = (0, 1)$  and  $k_3 = 2$  shown in figure 1.

( $\mathcal{L}_{A_1}, \mathcal{L}_{A_2}, \mathcal{L}_S$ ) differ, preventing explosive behaviour. The specific signs of these quantities for the examples illustrated in figure 1 are provided in table 1.

We have further validated these results by directly analysing the differential equation (5.5). By expressing  $S = |S|e^{i\vartheta}$ , we derive a system of second-order differential equations for  $S$  and  $\vartheta$ . Performing a double integration, along with a variable substitution  $v = |S|^2/2$ , reduces this to a single differential equation of the form

$$\frac{1}{2}\dot{v}^2 + \Pi(v) = 0, \tag{A2}$$

with  $\Pi(v)$  being the cubic potential

$$\Pi(v) = -4\alpha_1\alpha_2v^3 + \left[ \frac{(\beta_1 + \beta_2)^2}{4} + 2E_0 \right] v^2 - 2C_2v + \frac{C_1^2}{2}, \tag{A3}$$

where  $C_1$  and  $C_2$  are constants to be determined by imposing the initial conditions. As an example, the potential for the case with parameters  $n = (0, 1)$  and  $k_3 = 2$  is shown in figure 7. Following Craik (1988, pp. 137–138), the potential has three distinct real roots and its solution must oscillate in the potential well.

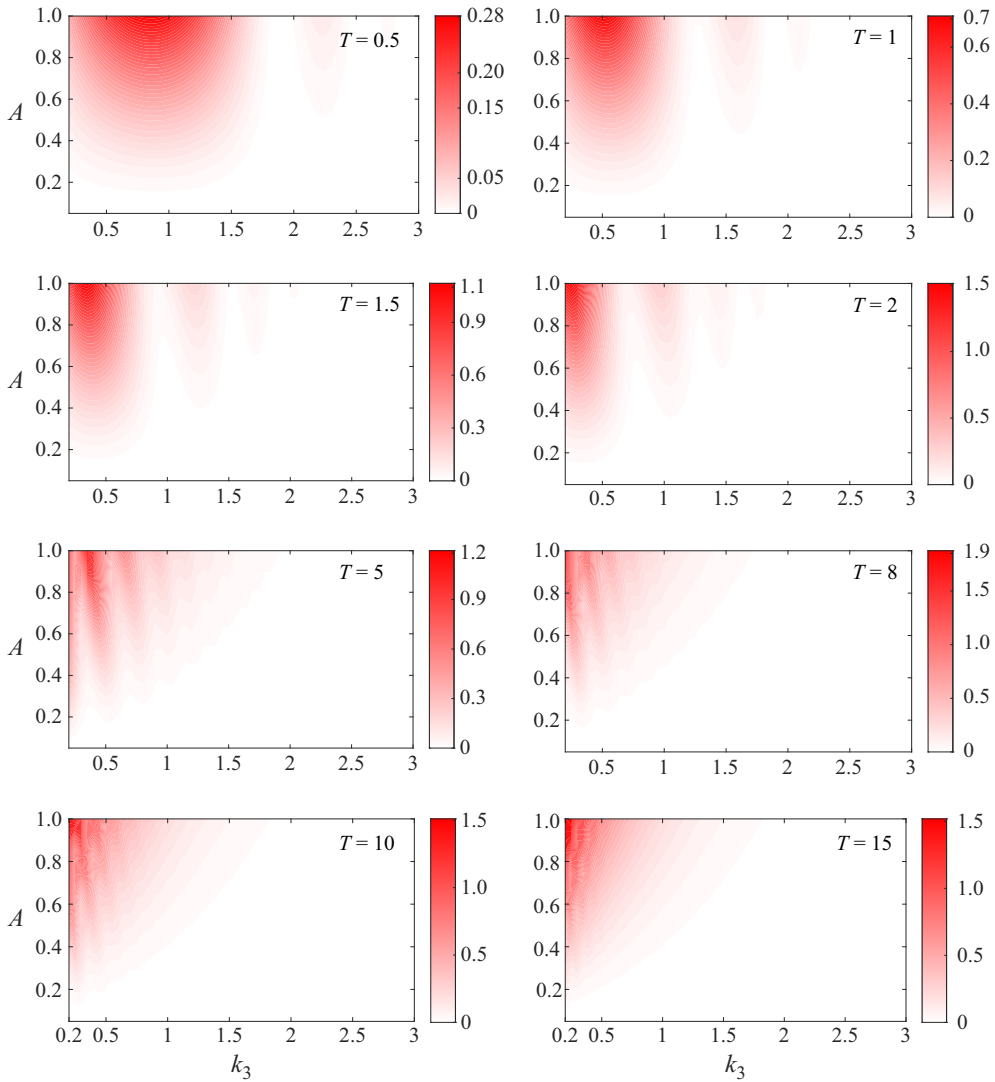


Figure 8. Difference function  $D_S$  for  $\sigma = 1$ ,  $n = (0, 0)$  and several times  $T$ , for the initial conditions (B1).

## Appendix B

Consider a single acoustic mode interacting with a gravity wave following the initial conditions

$$S(\xi, 0) = e^{-\xi^2}, \quad A_1(\xi, 0) = Ae^{-\xi^2}, \quad A_2(\xi, 0) = 0. \quad (\text{B1})$$

As a result of the interaction mechanism, a second acoustic mode is generated, which eventually influences the behaviour of the triad over longer time scales. In the current setting, no negative contours are observed, meaning that the amplitude of the initial surface gravity wave is either amplified or, at best, retained through interaction with a single initial acoustic mode (figure 8). This interaction also leads to the amplification of the second acoustic mode (the third member of the interacting triad) at the expense of the first acoustic mode (Kadri 2017). Specifically, part of the initial energy of the first acoustic mode is

transferred to both the gravity mode and the second acoustic mode, resulting in the latter's amplification.

REFERENCES

- ABRAMOWITZ, M. & STEGUN, I.A. 1965 *Handbook of Mathematical Functions: With Formulas, Graphs, and Mathematical Tables*. Dover Publications Inc.
- BALL, F.K. 1964 Energy transfer between external and internal gravity waves. *J. Fluid Mech.* **19** (3), 465–478.
- BENNEY, D.J. 1962 Non-linear gravity wave interactions. *J. Fluid Mech.* **14** (4), 577–584.
- BRETHERTON, F.P. 1964 Resonant interactions between waves. the case of discrete oscillations. *J. Fluid Mech.* **20** (3), 457–479.
- CRAIK, A.D.D. 1988 *Wave Interactions and Fluid Flows*. Cambridge University Press.
- CRUZ, J. 2007 *Ocean Wave Energy: Current Status and Future Perspectives*. Springer Science & Business Media.
- DUREY, M. & MILEWSKI, P.A. 2023 Resonant triad interactions of gravity waves in cylindrical basins. *J. Fluid Mech.* **966**, A25.
- EYOV, E., KLAR, A., KADRI, U. & STIASSNIE, M. 2013 Progressive waves in a compressible-ocean with an elastic bottom. *Wave Motion* **50** (5), 929–939.
- HAMMACK, J.L. & HENDERSON, D.M. 1993 Resonant interactions among surface water waves. *Annu. Rev. Fluid Mech.* **25** (1), 55–97.
- HASSELMANN, K. 1962 On the non-linear energy transfer in a gravity-wave spectrum: Part 1. general theory. *J. Fluid Mech.* **12** (4), 481–500.
- JOYCE, T.M. 1974 Nonlinear interactions among standing surface and internal gravity waves. *J. Fluid Mech.* **63** (4), 801–825.
- KADRI, U. 2016 Triad resonance between a surface-gravity wave and two high frequency hydro-acoustic waves. *Eur. J. Mech. ( B/ Fluids)* **55**, 157–161.
- KADRI, U. 2017 Tsunami mitigation by resonant triad interaction with acoustic–gravity waves. *Heliyon* **3** (1), e00234.
- KADRI, U. & AKYLAS, T.R. 2016 On resonant triad interactions of acoustic-gravity waves. *J. Fluid Mech.* **788**, R1.
- KADRI, U. & STIASSNIE, M. 2013 Generation of an acoustic-gravity wave by two gravity waves, and their subsequent mutual interaction. *J. Fluid Mech.* **735**, R6.
- KADRI, U. & WANG, Z. 2021 Approximate solution of nonlinear triad interactions of acoustic–gravity waves in cylindrical coordinates. *Commun. Nonlinear Sci.* **93**, 105514.
- LONGUET-HIGGINS, M.S. 1962 Resonant interactions between two trains of gravity waves. *J. Fluid Mech.* **12** (3), 321–332.
- LONGUET-HIGGINS, M.S. 1950 A theory of the origin of microseisms. *Phil. Trans. R. Soc. Lond. A Math. Phys. Sci.* **243** (857), 1–35.
- MANLEY, J.M. & ROWE, H.E. 1956 Some general properties of nonlinear elements-part i. general energy relations. *Proc. IRE* **44** (7), 904–913.
- MARTIN, R.A. & SEGUR, H. 2016 Toward a general solution of the three-wave partial differential equations. *Stud. Appl. Maths* **137** (1), 70–92.
- MCGOLDRICK, L.F. 1965 Resonant interactions among capillary-gravity waves. *J. Fluid Mech.* **21** (2), 305–331.
- MCGOLDRICK, L.F. 1970 An experiment on second-order capillary gravity resonant wave interactions. *J. Fluid Mech.* **40** (2), 251–271.
- MILES, J.W. 1976 Nonlinear surface waves in closed basins. *J. Fluid Mech.* **75** (3), 419–448.
- MULTON, B. 2013 *Marine Renewable Energy Handbook*. John Wiley & Sons.
- PHILLIPS, O.M. 1960 On the dynamics of unsteady gravity waves of finite amplitude part 1. the elementary interactions. *J. Fluid Mech.* **9** (2), 193–217.
- RASCLE, N. & ARDHUIN, F. 2013 A global wave parameter database for geophysical applications. part 2: model validation with improved source term parameterization. *Ocean Model.* **70**, 174–188.
- RASCLE, N., ARDHUIN, F., QUEFFEULOU, P. & CROIZÉ-FILLON, D. 2008 A global wave parameter database for geophysical applications. part 1: Wave-current–turbulence interaction parameters for the open ocean based on traditional parameterizations. *Ocean Model.* **25** (3-4), 154–171.
- RAUPP, C.F.M. & SILVA DIAS, P.L. 2009 Resonant wave interactions in the presence of a diurnally varying heat source. *J. Atmos. Sci.* **66** (10), 3165–3183.
- RAUPP, C.F.M., SILVA DIAS, P.L., TABAK, E.G. & MILEWSKI, P. 2008 Resonant wave interactions in the equatorial waveguide. *J. Atmos. Sci.* **65** (11), 3398–3418.

- SALAS, A.H. & CASTILLO, J.E.H. 2014 Exact solution to duffing equation and the pendulum equation. *Appl. Math. Sci.* **8** (176), 8781–8789.
- SCHIESSER, W.E. & GRIFFITHS, G.W. 2009 *A Compendium of Partial Differential Equation Models: Method of Lines Analysis with Matlab*. Cambridge University Press.
- SCHWARTZ, L.W. & VANDEN-BROECK, J.-M. 1979 Numerical solution of the exact equations for capillary-gravity waves. *J. Fluid Mech.* **95** (1), 119–139.
- SEGUR, H. 1980 Resonant interactions of surface and internal gravity waves. *Phys. Fluids* **23** (12), 2556–2557.
- SIMMONS, W.F. 1969 A variational method for weak resonant wave interactions, *Proc. R. Soc. A Math. Phys. Engng Sci.* **309**(1499), 551–575.
- TIAN, M. & KADRI, U. 2018 Wavemaker theories for acoustic-gravity waves over a finite depth. *J. Engng Maths* **108** (1), 25–35.
- WANG, Z., VANDEN-BROECK, J.-M. & MILEWSKI, P.A. 2013 Two-dimensional flexural-gravity waves of finite amplitude in deep water. *IMA J. Appl. Maths (Institute of Mathematics and Its Applications)* **78** (4), 750–761.
- WILLIAMS, B. & KADRI, U. 2023 On the propagation of acoustic-gravity waves due to a slender rupture in an elastic seabed. *J. Fluid Mech.* **956**, A6.
- WILTON, J.R. 1915 On ripples. *Phil. Mag.* **29** (6), 688–700.
- YANG, X., DIAS, F. & LIAO, S. 2018 On the steady-state resonant acoustic-gravity waves. *J. Fluid Mech.* **849**, 111–135.